Improved clouds over Southern Ocean amplify Antarctic precipitation response to ozone depletion in an earth system model

David P. Schneider, Jennifer E. Kay & Jan Lenaerts

Climate Dynamics
Observational, Theoretical and Computational Research on the Climate System

ISSN 0930-7575

Clim Dyn
DOI 10.1007/s00382-020-05346-8

Springer

Climate Dynamics
https://doi.org/10.1007/s00382-020-05346-8

Improved clouds over Southern Ocean amplify Antarctic precipitation response to ozone depletion in an earth system model

David P. Schneider[1,2] · **Jennifer E. Kay**[2,3] · **Jan Lenaerts**[3]

Received: 8 January 2020 / Accepted: 21 June 2020

Abstract
Increasing precipitation on the Antarctic Ice Sheet (AIS) in a warming climate has the potential to partially mitigate Antarctica's contribution to sea level rise. We show that a simple, physically motivated change to the shallow convective cloud phase in the Community Earth System Model (CESM)—improving a long-standing bias in shortwave cloud forcing over the Southern Ocean—leads to an enhanced response of precipitation when the model is forced with realistic stratospheric ozone depletion, with other radiative forcing remaining constant. We analyze two ozone-forced ensemble experiments with the CESM version 1.1: one using the standard version of the model and the other using the cloud-modified version. The standard version exhibits a precipitation increase on the AIS of 34 gigatons year^{-1}; the cloud-modified version shows an increase of 109 Gt year^{-1}. The cloud-modified version shows a more robust, year-round poleward shift in the westerly jet and storm tracks, which brings more precipitation to the AIS, compared to the standard version. Greater surface warming and larger-amplitude stationary waves further increase the Antarctic precipitation response. The enhanced warming in the cloud-modified version is explained by larger positive shortwave cloud feedbacks, while the enhanced poleward jet shift is associated with a stronger meridional temperature gradient in the upper troposphere—lower stratosphere. These results illustrate (1) the sensitivity of forced changes in Antarctic precipitation to the mean state of a climate model and (2) the strong role of atmospheric dynamics in driving that forced precipitation response.

Keywords Antarctic ice sheet · Precipitation · Shortwave cloud feedbacks · Structural uncertainty

1 Introduction

An estimated 6 mm of sea level equivalent, or over 2000 Gt, falls as snow on the grounded Antarctic ice sheet (AIS) and its major ice shelves each year. As such, any significant change in snowfall on the AIS, the dominant component of the surface mass balance (SMB), will significantly affect global sea level. In a warming climate, Antarctic snowfall is expected to increase due to the higher moisture holding capacity of the atmosphere with warmer air temperatures, and the accelerated hydrologic cycle. Despite a modest warming trend over the Antarctic continent since the 1950s (e.g. Steig et al. 2009; Nicolas and Bromwich 2014; Jones et al. 2019), there has been little observational evidence of an increase in Antarctic precipitation or SMB, either for the period since 1950 (Monaghan et al. 2006), or for the better observed period since 1979 (e.g. Lenaerts et al. 2012). These studies have been hampered by a sparse observational network, which, combined with difficulties in measuring snowfall, and large interannual and spatial variability, make the detection of significant trends challenging. A recent and extensive compilation of ice core accumulation rates (Thomas et al. 2017) lengthens the Antarctic precipitation record back 1000 years, offering a long-term perspective on Antarctic precipitation variability. This study suggests that Antarctic SMB has increased at an average rate of 7 ± 0.13 Gt/year per decade since 1800, translating into a sea level reduction of -0.02 mm/decade. The gridded snowfall reconstruction of Medley and Thomas (2019) refines the estimate of long-term SMB change, suggesting

✉ David P. Schneider
dschneid@ucar.edu

[1] Climate and Global Dynamics Laboratory, National Center for Atmospheric Research, Boulder, CO, USA

[2] Cooperative Institute for Research in Environmental Sciences, University of Colorado – Boulder, Boulder, CO, USA

[3] Department of Atmospheric and Oceanic Sciences, University of Colorado – Boulder, Boulder, CO, USA

Published online: 08 July 2020

that increased snowfall on the AIS has mitigated sea level rise by ~ 10 mm since 1901. Thus far, such evidence for increased snowfall has not been incorporated into assessments of AIS mass balance trends for the past few decades, since increased snowfall is not simulated by atmospheric reanalyses or derived regional climate model products (Lenaerts et al. 2019). The IMBIE team (2018) finds an average mass loss of 109 ± 56 Gt/year, which is almost entirely driven by ice dynamics, accompanied by an insignificant Antarctic-wide SMB change.

Models contributing to the Coupled Model Intercomparison Project, Phase 5 (CMIP5) on average project an increase in Antarctic precipitation of 25% by 2100 under a high emission scenario (RCP 8.5), translating into a cumulative sea level rise offset of 71 mm during the 21st century (Palerme et al. 2016). The multi-model average precipitation increase masks a large inter-model spread in Antarctic precipitation projections, which ranges from almost zero sea level rise offset to an offset of nearly 180 mm during the 21st century (Palerme et al. 2016). One explanation for this spread is a dependency on the models' present-day simulated sea ice area or extent (e.g. Agosta et al. 2015; Bracegirdle et al. 2015), which itself varies widely (e.g. Zunz et al. 2013). These studies (Agosta et al. 2015; Bracegirdle et al. 2015) argue that models starting out with greater sea ice extent warm faster, with more evaporation from the ocean and greater moisture transport to the AIS due to positive feedbacks between sea ice decreases and air temperature increases (i.e., the ice-albedo feedback mechanism). CMIP5 models do not show a consistent temperature-precipitation relationship (Palerme et al. 2016), possibly again due to their different initial sea ice states (Bracegirdle et al. 2015). Others have related projected precipitation trends to model resolution, namely models with finer horizontal resolution tend to produce larger increases in precipitation (Genthon et al. 2009). Some have suggested that the spread in precipitation projections largely reflects internal variability (Previdi and Polvani 2016). We note here that even if the models suggest that internal variability dominates over the forced signal, it does not mean that the models are free from flaws or biases. The roles of internal variability and structural (model) uncertainty in the intermodel spread of a given variable are difficult to disentangle in a multi-model ensemble such as CMIP5.

The central question of this study is whether the response of Antarctic precipitation to external forcing is sensitive to mean-state biases exhibited by a coupled Earth System model. One of the most prominent biases exhibited by many models is too-weak shortwave cloud forcing (SWCF), which results in an excess of absorbed shortwave radiation (ASR) over the Southern Ocean (e.g. Trenberth and Fasullo 2010; Schneider and Reusch 2016). This has numerous implications for the mean-state climate, including sea surface temperature (SST) biases (Schneider and Reusch 2016), ocean buoyancy (Sallée et al. 2013), and even the latitude and strength of the atmospheric jet (Ceppi et al. 2012). Here, we investigate structural uncertainty using the single model framework of the Community Earth System Model (CESM), version 1.1 (hereafter, CESM1; Hurrell et al. 2013). The standard version of the model, like many CMIP5 models, has a substantial mean-state ASR bias of ~ 20 W/m^2 over the domain of 40°S–60°S in the austral summer (Schneider and Reusch 2016). Kay et al. (2016) have introduced a modification to the shallow convection scheme of the atmospheric model component of CESM1, improving the radiative properties of clouds and substantially reducing the ASR bias over the Southern Ocean.

The implications of improving the radiative properties of Southern Ocean clouds for Antarctic climate projections have yet to be fully determined. Frey et al. (2017) evaluate the cloud-modified version of CESM1 (hereafter called 'CLDMOD') in comparison with the standard version for historical (1920–2005) and future (RCP8.5; 2006–2100) integrations. The standard version is that used for the CESM1 Large Ensemble Project (Kay et al. 2014); hereafter we refer to this as the 'LENS' version. For global surface temperature out to 2100, the single CLDMOD integration of Frey et al. (2017) lies near the upper bound of the 40-member LENS ensemble, but within the ensemble spread. Frey et al. (2017) did not evaluate Antarctic climate in detail, but noted that a stronger positive shortwave cloud feedback in CLDMOD over the mid-latitudes of the Southern Ocean results in greater warming of SSTs. However, efficient heat uptake by the mean overturning circulation of the Southern Ocean lessens the impact of the modified clouds on the global surface temperature as shown in Frey et al. (2017). Adopting the same benchmarks and methods as Schneider and Reusch (2016), we find that the historical CLDMOD simulation of Frey et al. (2017) has an austral summer ASR positive bias of ~ 5 W/m^2 over the Southern Ocean (40°S–60°S), a substantial reduction from the 20 W/m^2 bias exhibited by the standard version.

The goal of this study is to understand the implications of reducing the ASR bias on Antarctic climate change simulations by comparing experiments with CLDMOD and LENS. Given the central role of clouds and ASR in the surface energy budget of the Southern Ocean and Antarctica, it may be expected that changes to the Southern Ocean cloud properties will have a greater impact on local Antarctic climate than globally. Here we examine the role of structural differences between CLDMOD and LENS in the response to ozone depletion, which has been shown to be one of the main drivers of Southern Hemisphere climate change in recent decades (Polvani et al. 2011). For example, the impacts of ozone loss on atmospheric circulation are broadly consistent across a range of models (e.g. Eyring et al. 2013), and

a recent study (Lenaerts et al. 2018) showed ozone depletion to have a strong signature in Antarctic precipitation change in the CESM1. In addition, the response to ozone depletion is seasonal, while the ASR bias is also seasonal: Thus, if there are significant differences in the response to external forcing between CLDMOD and LENS, we should see these differences in experiments with strong, seasonal forcing whose response overlaps with the same season of the ASR bias. Like Lenaerts et al. (2018), we find an increase in Antarctic precipitation in response to ozone loss, and further show that improved clouds enhance this response due to both thermodynamic and dynamical mechanisms.

2 Models and methods

All experiments evaluated in this study are conducted with the CESM 1.1, configured with interactive ocean, atmosphere, sea ice and land component models (Hurrell et al. 2013). The ocean and sea ice model are on a ~ 1° grid, while the atmosphere and land models are on a 0.9° latitude × 1.2° longitude grid. This version of CESM1 has been extensively evaluated and used in a variety of applications, including CMIP5 experiments and the CESM1 Large Ensemble (CESM1-LE; Kay et al. 2014). Of particular relevance here is the model's performance in the Antarctic. This has been evaluated by Lenaerts et al. (2016), showing that CESM1 reasonably simulates the large-scale features of Antarctic climate, including present-day sea ice extent, major atmospheric circulation patterns, and the spatial distribution of surface temperatures and SMB on the ice sheet. Out of 41 CMIP5 models, Agosta et al. (2015) determine CESM1 to be the third-best model for Antarctic SMB simulations. Concerning biases in CESM1.1 include the excessive ASR noted above and a deficit in downward longwave and net surface longwave radiation on the AIS in austral winter (Lenaerts et al. 2016; Schneider and Reusch 2016). These features are characteristic of the 'LENS' version of CESM1.

The 'CLDMOD' version of CESM1.1 refers to the modifications to atmospheric component of the model, CAM5, discussed in Kay et al. (2016). Kay et al. (2016) modify the shallow convection detrainment, increasing supercooled cloud liquid and brightening low-level clouds. The substantially reduced Southern Ocean ASR bias cools the Southern Ocean, strengthens the mid-latitude westerly winds, and increases poleward heat transport. Other relevant changes to the climatology of the model, including increased ASR in the tropics, are discussed in Sect. 3.1.

Results presented here are based upon four distinct experiments (Table 1), all conducted with the CESM1-LE code base: (1) the pre-Industrial (1850) fully coupled control simulation for the CESM1-LE (Kay et al. 2014); (2) the pre-Industrial (1850) control run with the CLDMOD version of the model (Kay et al. 2016); (3) a "low ozone" 10-member ensemble with the LENS version; and (4) a "low ozone" 10-member ensemble with the CLDMOD version. The control simulations have preindustrial forcing that generally follows the CMIP5 protocol. A key deviation from CMIP5 protocol is that ozone forcing in our experiments is from simulations of the CESM1-Whole Atmosphere Community Model (WACCM; Marsh et al. 2013), a coupled chemistry-climate model which calculates ozone concentrations on the basis of prescribed ozone depleting substances. The CLDMOD control simulation was initialized from year 402 of the CESM1-LE control with identical external forcing, and integrated for 400 years.

The "low ozone" experiments have the same preindustrial (1850) radiative forcing as the control simulations, except that the 1850s ozone climatology is replaced with an ozone climatology based on the years 1996–2005 from the WACCM data set. Both climatologies only vary on a monthly basis: therefore, each year has the same ozone concentration in a given month. Ten ensemble members, each about 50 years long, are integrated for the LENS and the CLDMOD versions of the model. The LENS low ozone ensemble is initialized at year 1601 of the CESM1-LE control; the CLDMOD low ozone ensemble is initialized at year 300 of the CLDMOD control. The ensemble spread in both ensembles is generated by the pertlim parameter in the atmosphere model; this slightly perturbs the initial atmospheric conditions of each ensemble member on the first day of the simulation. It is the same protocol followed to generate the ensemble members of the CESM1-LE.

Table 1 Experiments discussed in this study and forcing details

Experiment	Ozone forcing	Kay et al. (2016) cloud modifications?	Other external forcing	Ensemble members
1850 LENS pre-Industrial (PI) control	1850s WACCM climatology	No	1850s PI climatology	1 (2000 years)
1850 CLDMOD PI control	1850s WACCM climatology	Yes	1850s PI climatology	1 (400 years)
1850 LENS PI control + low ozone	1996–2005 WACCM climatology	No	1850s PI climatology	10 (51 years each)
1850 CLDMOD PI control + low ozone	1996–2005 WACCM climatology	Yes	1850s PI climatology	10 (51 years each)

We note that we would expect similar results with single runs of 500 years each instead of 10 runs of 50 years each. Here, we have adopted the ensemble approach because an additional application of these experiments, beyond those discussed in this paper, is to evaluate the "fast" and "slow" responses to ozone depletion, and isolating the fast response requires a relatively large ensemble (Ferreira et al. 2015). In this paper, we focus on the slow, long-term response. In the CESM1, the crossover time from the fast to slow response occurs within about four years of a step increase in the wind speed over the Southern Ocean (Kostov et al. 2016).

The prescribed ozone forcing is illustrated in Fig. 1, which shows the difference of the 1996–2005 ozone climatology and the 1850 ozone climatology averaged over 60°S–90°S as a function of month and height. The largest changes occur in October through December, between 100 and 70 hPa, where over 70% ozone loss occurs. Greater than 40% ozone loss occurs down to ~ 200 hPa and between September and February. While polar stratospheric ozone loss is by far the largest forcing signal, there are also some modest increases in tropospheric ozone (up to 20% in the middle troposphere). The tropospheric changes lead to modest tropospheric warming in the middle and low latitudes, especially in the Northern Hemisphere. The use of the full column ozone changes rather than only those in the stratosphere ensures consistency with the CESM1-LE experiments and with the experiments of Lenaerts et al. (2018). Importantly,

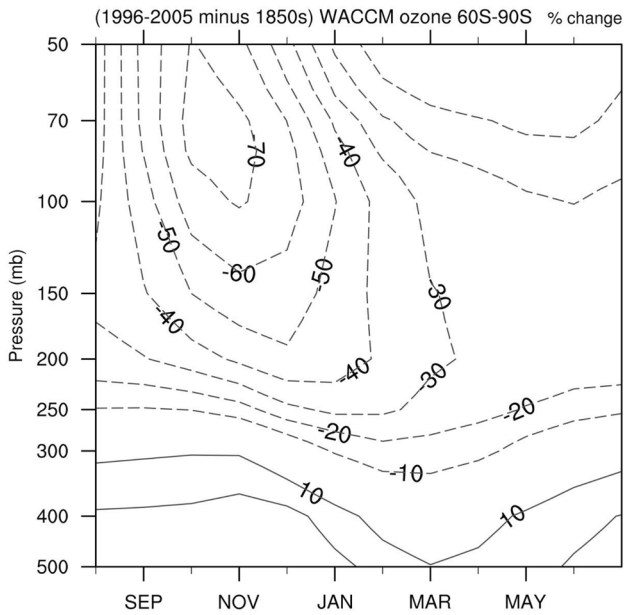

Fig. 1 The prescribed ozone forcing for the polar cap region (60°S–90°S) on a month-height plot, showing the percent difference in ozone concentration between the perturbed experiments (which have 1996–2005 ozone) and the control simulations (which have 1850s ozone). Negative contours (ozone depletion) are dashed; positive contours are solid; the interval is 10%

the goal of this paper is to evaluate the role of the structural differences between CLDMOD and LENS, rather than to have the most realistic forcing possible. Results from further CLDMOD experiments with realistic historical forcing, similar to the one discussed in Frey et al. (2017), will be presented in future work.

The response to ozone is defined as the difference of the "low ozone" ensemble and the control run for each version of the model (LENS and CLDMOD). For example, the response in CLDMOD is taken as the average over the ensemble mean (except where noted) of years 5–52 of the low ozone ensemble minus the average of years 305–352 of the control simulation. The first four years of the experiments are discarded in order to focus on the "slow" response to ozone forcing. The clearest results are found using the exact overlapping segment of the control run rather than an arbitrary segment of the control run, likely because this removes any signals of drift or low-frequency climate variability. The statistical significance of the responses are determined from a two-sided t test, with the sample size and variance of the low ozone experiments calculated on the basis of all ensemble members. That is, the 45-year segments of 10 ensemble members are appended to each other to calculate the mean, variance and sample sizes that are applied in the t test statistic. The next section of this paper describes the results, first explaining the major climatological differences between the LENS and CLDMOD versions of the model, and then discussing the major features of the response to ozone depletion in both versions of the model. Finding a significant difference in the precipitation responses over the AIS, we then discuss the reasons for this difference and the role of atmospheric circulation and thermodynamics. Differences in the shortwave cloud feedbacks between the two models are also analyzed and discussed. Finally, Sects. 4 and 5 provide a Discussion and concluding remarks.

3 Results

3.1 Climatological differences between LENS and CLDMOD

The first set of results, augmenting those discussed in Kay et al. (2016), highlights the structural differences between the LENS and CLDMOD versions of the model. In the middle to high latitudes of the Southern Hemisphere, the CLDMOD control simulation is colder, windier, and drier than the LENS control simulation (Figs. 2, 3 and 4). Due to the seasonal cycle of insolation, the largest cloud-driven differences occur in austral summer (not shown). Figure 2 illustrates the surface temperature and 500 hPa geopotential height differences in DJF. In CLDMOD, nearly all of the Southern Ocean is colder by 0.5° to 2 °C, except for two

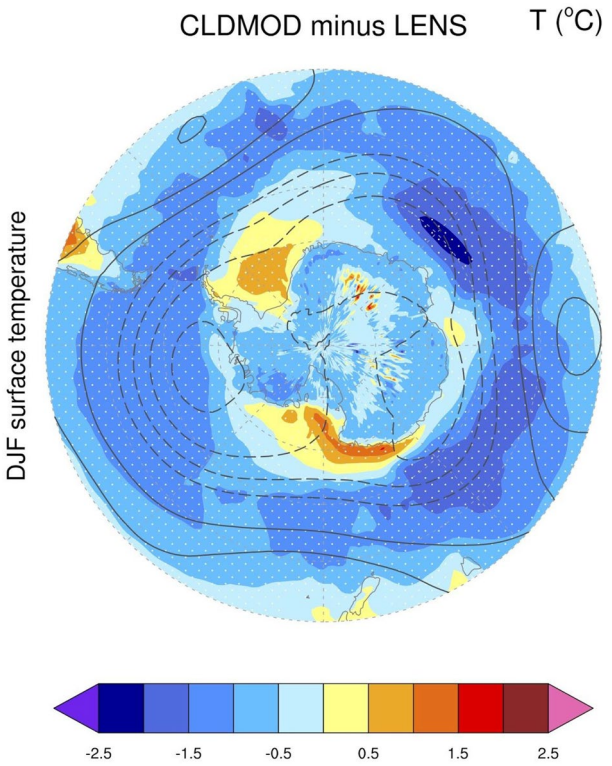

Fig. 2 Difference in surface temperature (colors) and 500-hPa geopotential height (contours) between the CLMOD and LENS 1850 control simulations for DJF. The negative contours are dashed and the positive contours are solid; the interval is 8 m

areas near the Antarctic coast. Geopotential height differences resemble the positive phase of the Southern Annular Mode, with lower heights over the middle and high latitudes, consistent with a stronger westerly jet. The stronger jet is evident in the zonal mean in Fig. 3b. The jet strengthens more than it shifts in latitude. This is driven by warming in the tropics and cooling in the high latitudes (Fig. 3a), creating a stronger meridional temperature gradient and increasing zonal wind speed via the thermal wind relationship. The enhanced meridional temperature gradient arises from the brightening of clouds over the Southern Ocean and the dimming of clouds in the tropics (Kay et al. 2016). The pattern of warming in the tropical and subtropical upper troposphere, and weak cooling in the polar lower stratosphere, is suggestive of an increase in tropopause height, as well as an increase in the meridional slope of the tropopause (e.g. Vallis et al. 2015). In the Southern Ocean latitudes, the largest cooling occurs in the lower troposphere, below 500 hPa to 700 hPa. The surface cooling and drying of the Southern Ocean in CLDMOD extend throughout the water column (not shown).

LENS has an annual mean snowfall integrated over the grounded AIS (excluding the ice shelves) of 1618 Gt year^{-1}, while CLDMOD has 1462 Gt year^{-1}, a reduction of about 10%. The interannual standard deviation of the annual mean snowfall is 71 Gt/year in LENS and 57 Gt/year in CLDMOD. The seasonal-mean precipitation for DJF (Fig. 4a) is reduced in CLDMOD across nearly all of the AIS (Fig. 4b, c). Across the Southern Ocean, the pattern of precipitation difference is not uniform, but rather shows distinct areas of increases and decreases. This is associated with the stationary wave pattern in the atmospheric circulation, which is overlaid on the precipitation pattern in Fig. 4c. Zonal wave-3 is more prominent in CLDMOD, creating regions of strong meridional flow, compared to LENS. Regions with the most significant precipitation decreases, especially in the eastern hemisphere, are associated with southerly flow from the polar regions to the middle latitudes (Fig. 4b). The areas of precipitation increase, while largely not statistically significant, are associated with northerly flow. While the overall reduction of precipitation in CLDMOD is consistent with the colder atmosphere and ocean, the precipitation differences between CLDMOD and LENS are also driven by the atmospheric circulation differences. The influence of circulation can be seen to some extent in the patterns of interannual variability. As discussed in Fyke et al. (2017), the spatial pattern of the interannual standard deviation in LENS (Fig. 4d) generally follows the pattern of the mean. Coastal areas with large seasonal-mean precipitation have high standard deviations, while interior areas with low precipitation have low standard deviations. Although this pattern is largely similar in CLDMOD (not shown), there are differences in the relative patterns of variability. The coefficient of variation (the standard deviation divided by the mean), is shown in Fig. 4e, f. CLDMOD generally has slightly higher values, especially in East Antarctica between 135°E and 170°E, and in West Antarctica on either side of the divide. These are regions where the stationary waves penetrate into the interior of the continent.

The reduction of the SWCF and ASR biases, the less zonally symmetric circulation pattern, and the lower summer SSTs in CLDMOD compared to LENS alleviate some of the shortcomings in CESM1′s simulation of Antarctic climate (e.g. Lenaerts et al. 2016; Schneider and Reusch 2016). In contrast, the strengthening of the jet, increase in sea ice extent, and the reduction in precipitation on the AIS reinforce existing known biases (Kay et al. 2016; Lenaerts et al. 2016). Taken together, these contrasts between CLDMOD and LENS illustrate that the two versions of the model are structurally different, a fact that we leverage to explore the sensitivity of precipitation responses to the mean-state climate of the model.

3.2 Atmospheric circulation and temperature responses to ozone depletion

The expected signature of polar stratospheric ozone depletion is a sharp cooling of the lower stratosphere during the spring and summer, accompanied by a lowering of

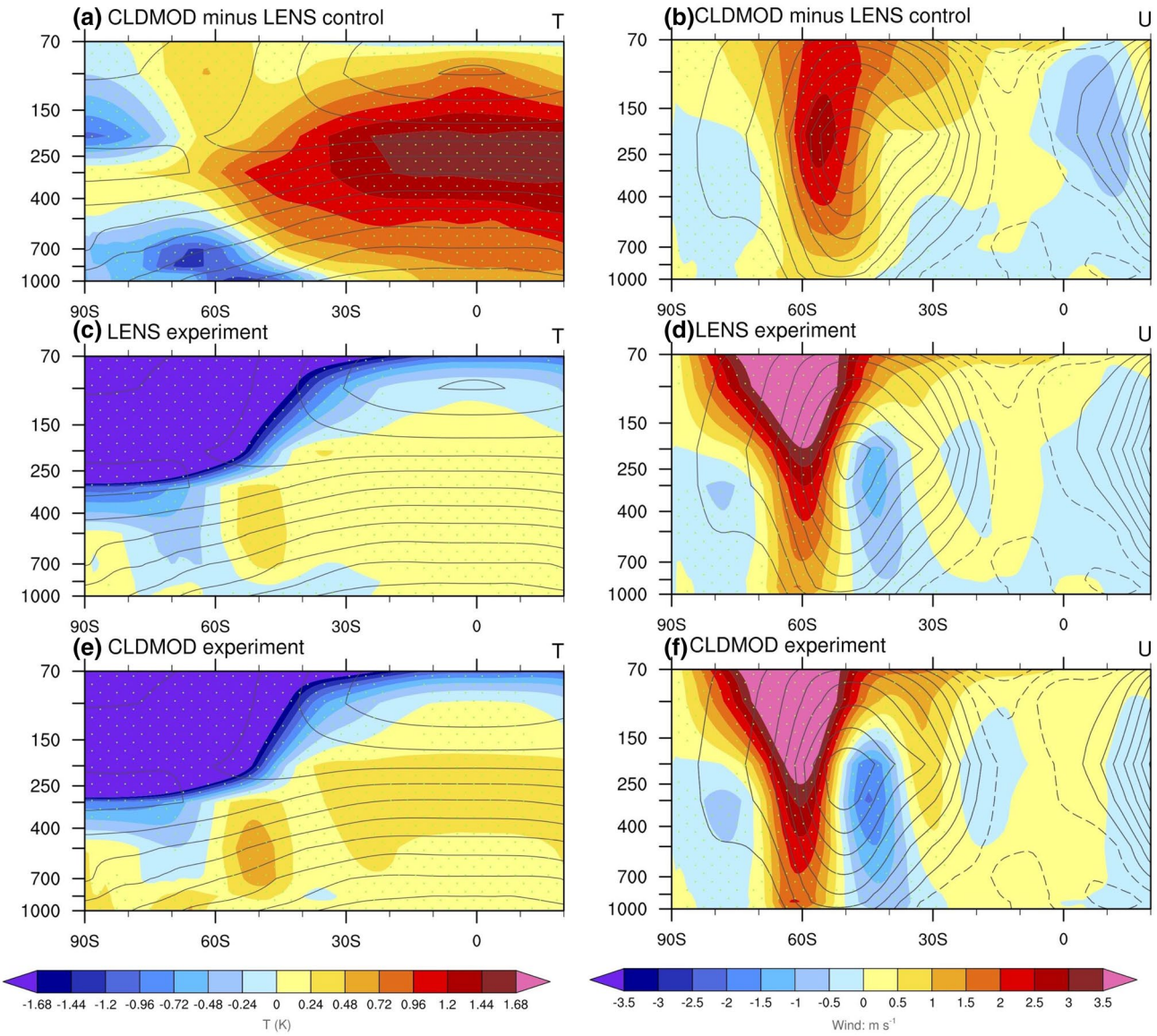

Fig. 3 Climatological difference between control simulations for zonal-mean **a** temperature and **b** wind for DJF. Response of zonal-mean temperature (**c**, **e**) and wind (**d**, **f**) in DJF to ozone depletion for the LENS (**c**, **e**) and CLDMOD (**d**, **f**) experiments. The climatology from the respective control simulations is shown as contours (temperature contoured at 10 °C; wind contoured at 4 m/s). Temperature or wind responses that are statistically significant are indicated with green stippling

geopotential height over the polar cap (e.g. Gillett and Thompson 2003). Figure 5 demonstrates that this first-order response to ozone loss is robust and consistent across the LENS and CLDMOD experiments. The maximum stratospheric cooling of 10 °C to 12 °C occurs at about 70 hPa in November to December in both models. Recall from Fig. 1 that the ozone loss itself peaks in October to November, so the peak cooling is delayed by about a month. The peak cooling propagates with time to lower levels, where it is of weaker magnitude but more persistent. Between 200 hPa and 250 hPa, cooling of 4 °C starts in December and persists through February. Cooling of at least 1 °C persists until May. We note that seasonal stratospheric cooling begins a bit earlier in CLDMOD: As seen in Fig. 5b, the 2 °C contour appears in August to September above 70 hPa. In both models, the maximum geopotential height response in the stratosphere at 70 hPa occurs in December. Unlike temperature, the geopotential response does not propagate downward with time; the maximum response at 250 hPa also occurs in December. A response of at least 20 m extends into the mid-troposphere in December and January.

Having established that both versions of the model behave in the expected, canonical way in response to stratospheric ozone depletion and that the largest responses in

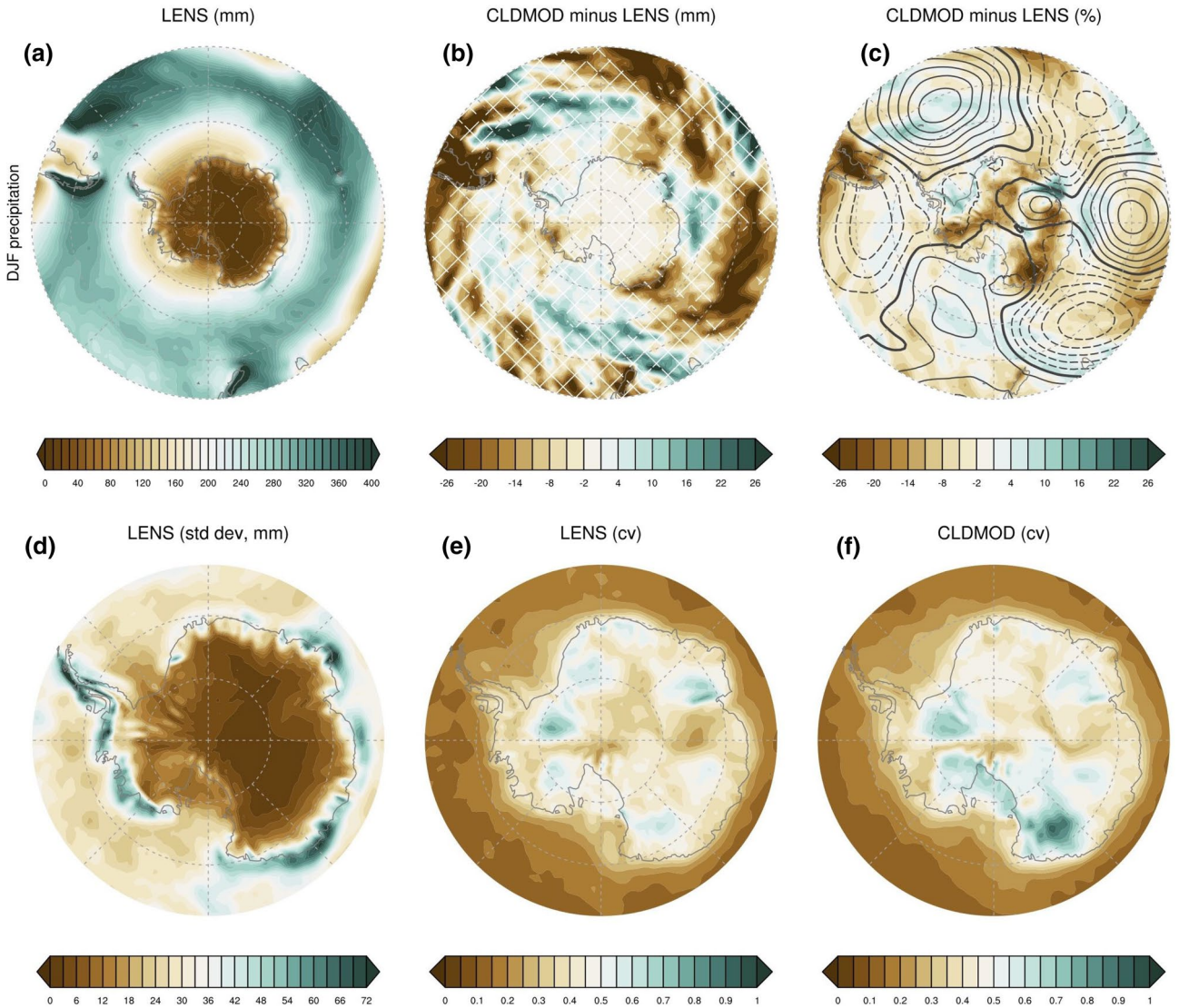

Fig. 4 **a** The seasonal-mean precipitation in DJF in the LENS control simulation in mm water equivalent; **b** the absolute difference in DJF precipitation between the CLDMOD and LENS control runs (hatched areas are insignificant differences); and **c** the percentage difference in DJF precipitation between CLDMOD and LENS control runs. Also shown in (**c**) is the difference in the stationary wave pattern at 500 hPa, contoured at an interval of 2 m with negative values dashed and positive values solid. **d** The interannual standard deviation of the seasonal-mean precipitation in LENS; **e** the coefficient of variation (cv) in LENS; **f** the coefficient of variation (cv) in CLDMOD (see text for details)

the troposphere occur in December through February, we now highlight the seasonal-mean responses in DJF. Later, we shall return to the annual mean perspective, as this has the most direct implications for the overall mass balance of the AIS, and shows the primary reasons for the differences in the precipitation responses of CLDMOD and LENS. Taking a zonal-mean view, Fig. 3c–f shows the temperature and wind responses for the entire Southern Hemisphere. Here we begin to see some differences between the LENS and CLDMOD responses, especially in the troposphere (the color bars are scaled to emphasize the troposphere). While the overall patterns of the responses are similar, tropospheric warming is generally about 0.1 °C to 0.2 °C greater in CLDMOD than in LENS. In both model versions, the maximum tropospheric warming occurs at 50°S and between 500 hPa and 700 hPa. Near the surface, and between 30°S and 60°S, zonal-mean cooling occurs in LENS while warming occurs in CLDMOD. The zonal wind speed increases in both model versions on the poleward side of the climatological jet, and decreases on the equatorward side—the signature of a poleward shift in the latitude of the jet. In addition, the zonal wind anomalies amplify with height on the poleward side of the jet, which is a characteristic response to stratospheric ozone depletion (e.g. Schneider and Deser 2015). These

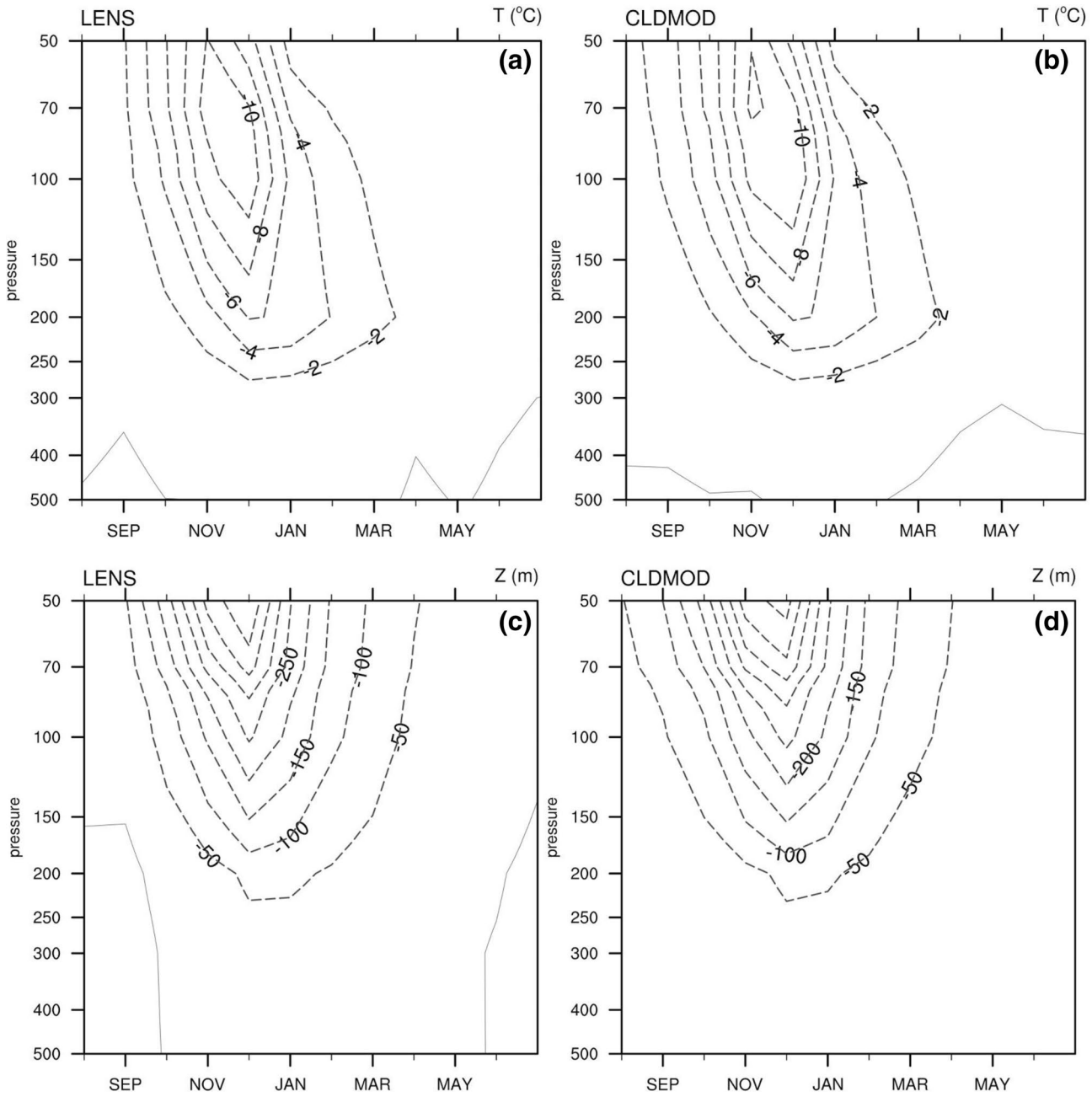

Fig. 5 Month-height plots showing responses of temperature and geopotential height over the polar cap region (60°S–90°S) to ozone depletion. **a** temperature response in LENS; **b** temperature response in CLDMOD; **c** geopotential height response in LENS; **d** geopotential height response in CLDMOD. The contour interval is 2 °C for temperature and 50 m for geopotential height; negative contours are dashed

wind speed changes are somewhat stronger in CLDMOD compared to LENS. Near the surface, the nodal latitude between the increase and decrease in wind speed is shifted about 2° poleward in CLDMOD compared to LENS.

Differences in the surface temperature responses are even more apparent in map view (Fig. 6). As seen in Fig. 6a, there is a large region of significant cooling across the Southern Ocean in LENS; cooling occurs over a much smaller surface area in CLDMOD (Fig. 6b). Warming in both models is greatest in the Atlantic sector, locally reaching greater than 0.5 °C in CLDMOD but only 0.25 °C to 0.3 °C in LENS. In the Pacific sector to the east of New Zealand, there is significant cooling of − 0.2 °C to − 0.4 °C in LENS, in contrast with significant warming of 0.2 °C to 0.5 °C in CLDMOD. Over the AIS, significant surface cooling in parts of East Antarctica, between 90°E and 135°E in LENS, is absent in

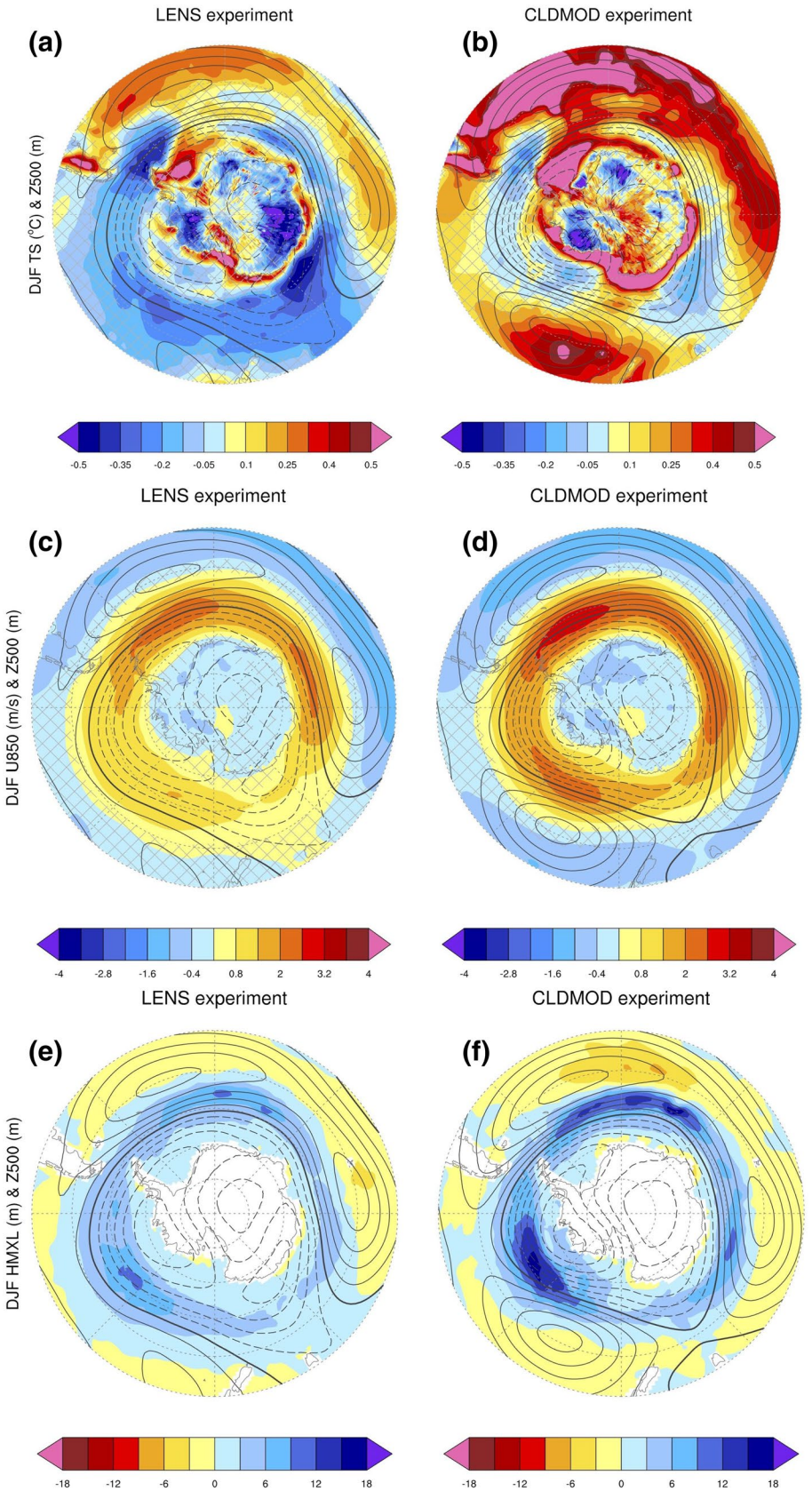

Fig. 6 Maps of surface temperature, geopotential height, zonal wind, and mixed layer depth responses in DJF to ozone depletion. **a** Temperature (colors) and 500 hPa height (contours, interval 6 m) in LENS; **b** temperature (colors) and 500 hPa height (contours, interval 6 m) in CLDMOD; **c** 850 hPa zonal wind (colors) and 500 hPa height (contours, interval 6 m) in LENS; **d** 850 hPa zonal wind (colors) and 500 hPa height (contours, interval 6 m) in CLDMOD. Hatching indicates temperature or wind responses that are not statistically significant. **e** Mixed layer depth response in CLDMOD; **f** Mixed layer depth response in LENS (500 hPa height (contours, interval 6 m))

CLDMOD, but CLDMOD shows significant cooling in parts of West Antarctica.

The atmospheric circulation changes accompanying the temperature responses are also displayed in Fig. 6. The 500 hPa geopotential height response is shown in all panels as contours; the 850 hPa zonal wind response is shown in the lower panels as colors. The zonal wind response is more intense in CLDMOD, and the westerly wind increase is more narrowly confined to the high latitudes, compared to LENS. The pattern is also more zonally symmetric, owing to the prominent anticyclonic circulation center at 50°S, 150°W that is absent in LENS. The two anticyclonic circulation cells in the Atlantic and Indian Ocean sectors at 50°S are about 6 m stronger in CLDMOD.

Comparing the zonal wind response (Fig. 6c, d) with the temperature response (Fig. 6a, b), it can be seen that areas of significant warming correspond to those of significant zonal wind speed decreases. The areas of largest warming are located on the northern sides of the three anticyclonic circulation cells centered at 50°S, suggesting that some of the warming is circulation induced. In addition, weaker surface winds correspond with negative mixed layer depth anomalies, as seen in Fig. 6e, f. From observational studies (e.g. Sallée et al. 2010), negative mixed layer depth anomalies in the Southern Ocean mid latitudes imply positive SST anomalies, less entrainment of water from the ocean interior into the mixed layer, and greater stratification of the water column. While the analysis of each of these processes is beyond the scope of this study, the general relationships between wind anomalies, SST anomalies, and mixed layer depth anomalies are clearly evident in the model (Fig. 6). However, the magnitudes of the mixed layer depth response in these experiments are much smaller than those observed in association with modes of variability such as the Southern Annular Mode (e.g. Sallée et al. 2010), and the differences between CLDMOD and LENS are not very large. Below, we will consider other processes, including Ekman and surface heat fluxes, and, most importantly, shortwave cloud feedbacks, which better explain the difference in SST and air temperature differences between CLDMOD and LENS.

While the circulation responses are broadly zonally symmetric, with positive heights in the middle latitudes and negative heights at lower latitudes, the patterns are also characterized by prominent stationary waves. Figure 7 shows the stationary wave patterns at 500 hPa in CLDMOD and LENS, while Table 2 shows the maximum amplitudes of zonal wavenumbers 1, 2, and 3 for 50°S–70°S and 70°S–90°S. In LENS, the response projects most strongly on to zonal wave-1, which weakens by 13 m over the ocean and strengthens by 5 m over the AIS. Over the ocean, this is marked by a trough between about 100°E and 60°W, and a ridge between 60°W and 100°E (Fig. 7a). Embedded within this large-scale ridge-trough structure, the wave 3 pattern strengthens by 5 m over the ocean. Over the AIS, the stationary wave response

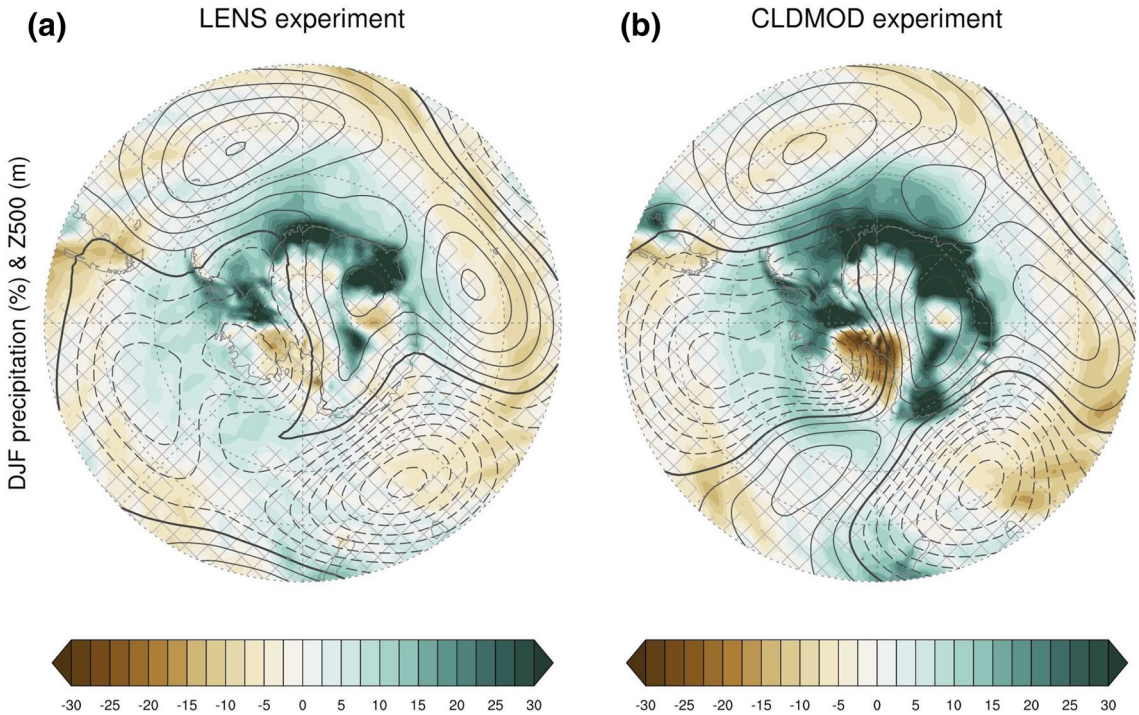

Fig. 7 Maps of the precipitation (colors, percent) and stationary waves at 500 hPa (contours, interval 3 m) responses in DJF to ozone depletion in **a** LENS and **b** CLDMOD. Hatching indicates statistically insignificant precipitation responses

Table 2 Maximum stationary wave amplitude (meters) at 500 hPa and between 50°S and 70°S (70°S–90°S) in DJF in each experiment

Experiment	Wave1	Wave2	Wave3
1850 LENS PI control	69 (24)	14 (18)	36 (6)
1850 CLDMOD PI control	67 (23)	16 (18)	40 (6)
1850 LENS PI control + low ozone	56 (29)	13 (18)	41 (6)
1850 CLDMOD PI control + low ozone	59 (32)	19 (17)	47 (8)

is characterized by a trough over West Antarctica and a ridge over East Antarctica, a pattern created by the poleward movement of the jet interacting with the topography of the continent. In CLDMOD, the responses of zonal wave 1 and zonal wave 3 are approximately equal (7–8 m) over the ocean. This makes the amplitudes of zonal wave 1 and zonal wave 3 closer to each other: In the CLDMOD control simulation, zonal wave 1 is 17 m stronger than zonal wave 3; in the CLDMOD ozone experiment, zonal wave 1 is 12 m stronger than zonal wave 3. The relative amplification of zonal wave 3 contributes to areas of strong meridional circulation and explains the anticyclonic circulation response to the east of New Zealand. Over the AIS, wave 1 strengthens by 9 m in CLDMOD, marked by a sharp contrast in the circulation pattern between the EAIS and WAIS (Fig. 7b).

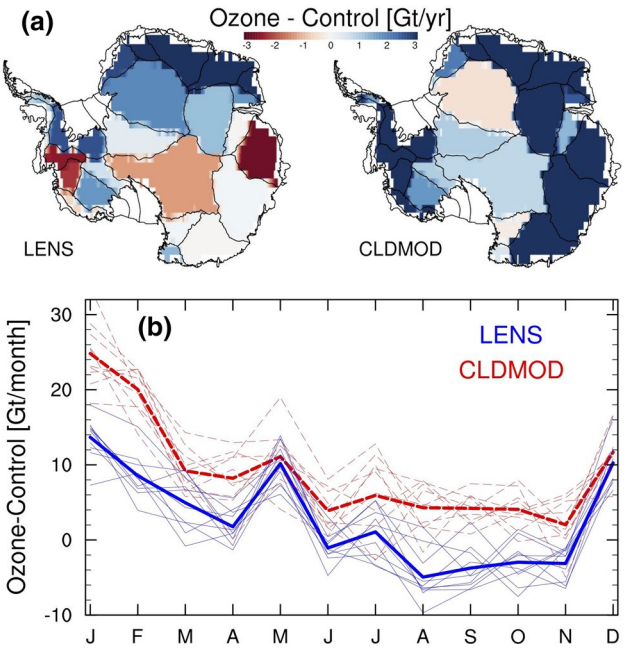

Fig. 8 **a** Maps of the annual-mean, ensemble-mean precipitation response to ozone depletion over the AIS, expressed as mass changes (Gt/year) in each glaciological basin for LENS (left panel) and CLDMOD (right panel); **b** Monthly precipitation response to ozone depletion averaged over the grounded AIS in each LENS (thin, solid blue curves) and CLDMOD (thin, dashed red curves) ensemble member, expressed as Gt/month; thick curves denote the ensemble means

3.3 Amplified precipitation response in CLDMOD

Having demonstrated that two structurally different versions of the CESM1 forced with identical ozone concentrations show somewhat different temperature and atmospheric circulation responses to ozone depletion, we now turn to the precipitation responses. Figure 7 shows the responses as a percentage of the pre-industrial climatology for DJF for the whole domain while Fig. 8a shows the absolute mass changes in each basin of the AIS for the annual mean. The DJF pattern in LENS is characterized by a dipole over the West Antarctic Ice Sheet (WAIS), with an increase in precipitation of up to 30% on the Peninsula and Ronne-Filchner Ice Shelf Region, and a decrease in precipitation in Marie Byrd Land and the Ross Ice Shelf region. Precipitation increases in coastal East Antarctica between 0°E and 90°E, and changes very little in the rest of the East Antarctic Ice Sheet (EAIS). In contrast, CLDMOD shows an increase in precipitation over all of coastal East Antarctica, and a stronger dipole across West Antarctica. Across the Southern Ocean, the precipitation response in both models has a zonal component to it, with decreases between 40°S and 55°S, and increases polewards of 60°S, consistent with the poleward movement of the storm track. However, the precipitation pattern deviates from zonal symmetry in some regions. For example, the trough centered south of Tasmania is associated with a meridional dipole in the precipitation response pattern. Dry anomalies are associated with southerly flow and positive anomalies are associated with northerly flow from the moisture-rich middle latitudes. Weaker dipole patterns are seen elsewhere, especially in CLDMOD with its larger-amplitude stationary waves.

Returning to the continent, the stationary wave structure with a ridge over the EAIS and trough over the WAIS (Fig. 7a, b), is reminiscent of the circulation patterns that drive large positive anomalies in moisture transport and Antarctic precipitation in the CESM1 (Fyke et al. 2017). Compositing the circulation anomalies associated with high precipitation years in each basin of the AIS in the LENS control simulation (the same control experiment used here), Fyke et al. (2017) found a strong relationship between ridging and positive precipitation anomalies in East Antarctic basins. Mechanistically, these circulation patterns, with meridionally oriented streamlines, facilitate the delivery of moisture from distant, oceanic sources to the AIS. As seen in Fig. 7, these circulation patterns are more prominent in the CLDMOD response than in the LENS response, again reflecting the larger stationary wave amplitudes in CLDMOD. In CLDMOD, the extent to which the circulation response leads to positive precipitation anomalies in most basins of the AIS is striking.

Figure 8a presents the annual-mean precipitation response for the grounded AIS. In total, the CLDMOD response is an increase of 109.6 Gt year^{-1} (or 7.5%) and the LENS response is an increase of 34.1 Gt year^{-1} (or 2.1%). A month-by-month integration (Fig. 8b) shows that the annual-mean increases are largely driven by the responses in December, January, and February in both CLDMOD and LENS. In December, the two ensemble means are close to each other, while in January and February, CLDMOD has about a 10 Gt larger response than LENS. Figure 8b further shows the responses in each ensemble member, revealing that the two ensembles are most distinct (no overlapping members) in January. However, the ~ 10 Gt amplification in CLDMOD in January and February does not explain the ~ 75 Gt (three-fold) amplification of the annual-mean response relative to LENS. From June thru October, the response in LENS is near zero to negative, offsetting the precipitation increases from December through May. In contrast, CLDMOD exhibits a precipitation increase in all months of the year in nearly every ensemble member, further adding to the large precipitation increases in December thru February.

The spatial patterns of the annual-mean precipitation responses (Fig. 8a) are similar to the DJF patterns (Fig. 7), underscoring the fact that the largest precipitation increases occur in DJF. Figure 9 further illustrates the significance of the DJF response, showing the zonal-mean precipitation response in each ensemble member together with the zonal-mean surface temperature and 850 h Pa zonal wind responses. For precipitation (Fig. 9a), the response is very consistent across both the LENS and CLDMOD ensemble members. Every ensemble member shows an increase polewards of 55°S, decreases between about 40°S and 55°S, and little change equatorwards of 40°S. The CLDMOD ensemble is clearly separated from the LENS ensemble over the coastal latitudes of the AIS (~ 65°S to 75° S). For surface temperature (Fig. 9b), all CLDMOD ensemble members warm at all latitudes between 35°S and 75°S, while the only consistent signal among the LENS members is cooling between 50°S and 65°S. For zonal wind (Fig. 9c), the responses are again consistent across all ensemble members of both CLDMOD and LENS, with a clear poleward shift from the mean jet latitude of ~ 50°S. This response is accentuated in CLDMOD, where all ensemble members exhibit stronger jet shifts then the LENS members.

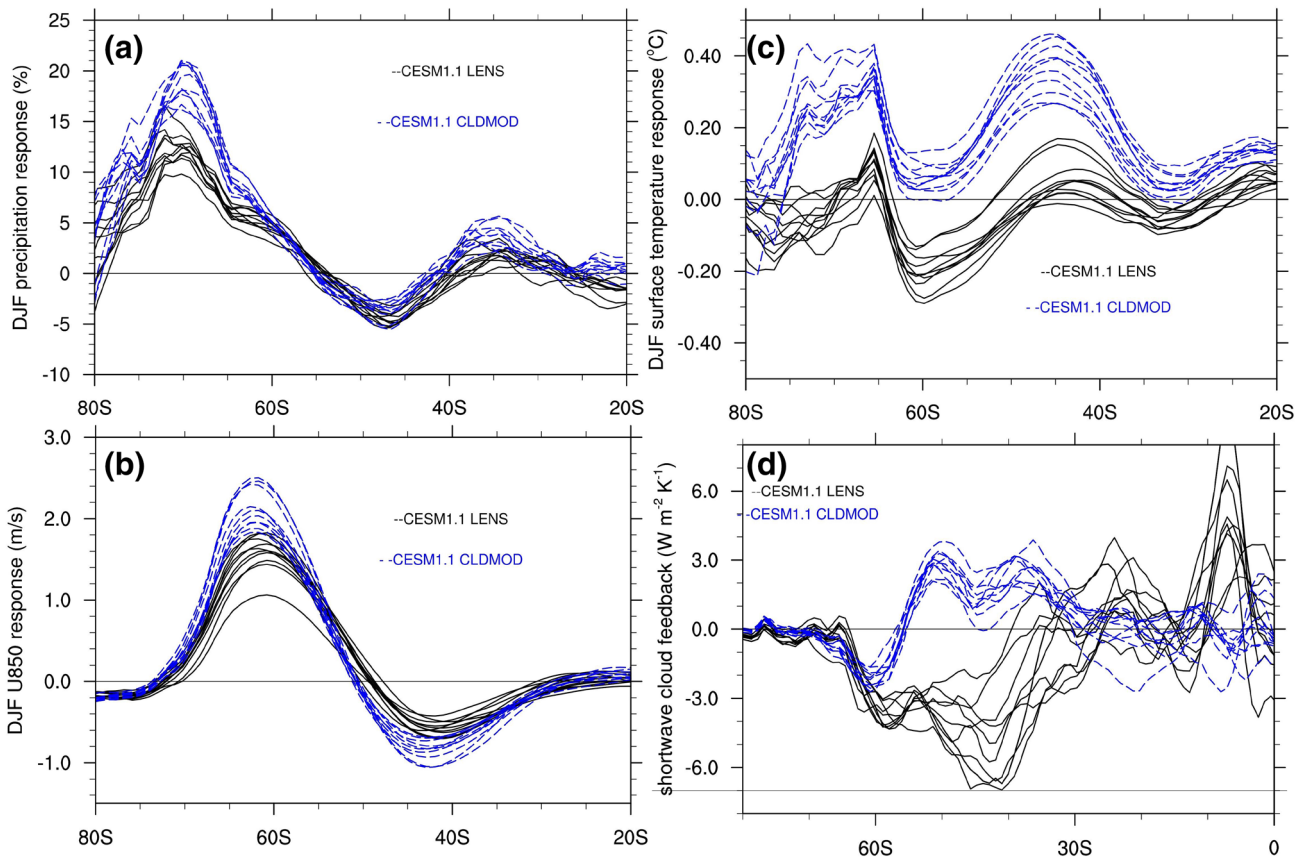

Fig. 9 Zonal-mean responses to ozone depletion for: **a** DJF precipitation; **b** DJF zonal wind at 850 hPa; **c** DJF surface temperature; **d** annual shortwave cloud feedback. Individual ensemble members are shown in black for LENS and blue for CLDMOD

3.4 Distinguishing between dynamic and thermodynamic precipitation responses

Thus far, the results have suggested two explanations for the larger Antarctic precipitation response in CLDMOD compared to LENS: (1) greater surface and atmospheric warming; and (2) a stronger poleward jet shift and intensification of the westerlies. To understand how these mechanisms work together, and which one may be the most important, we first evaluate how the precipitation response co-evolves with the atmospheric circulation and temperature responses through the seasonal cycle. Second, we evaluate the sensitivity of precipitation to temperature, the so-called temperature-precipitation slope, as this has been the major explanation for increased Antarctic precipitation in a warming climate. Recall from the discussion above that year-round processes are important to explain the amplified precipitation response in CLDMOD, not just austral summer processes.

Figure 10 shows the zonal-mean, month-by month evolution of the responses of precipitation, 850-hPa zonal wind, sea level pressure (SLP), and 850-hPa air temperature in LENS and CLDMOD for the latitudes 30°S–80°S. While maximized in austral summer, the precipitation increase in CLDMOD nonetheless occurs year-round polewards of 55°S, whereas the high-latitude precipitation increase in LENS happens only in the summer and autumn months, all of which confirm our results in Fig. 8b. The zonal wind and SLP responses likewise show a stronger seasonality in LENS than in CLDMOD. Both model versions exhibit maximum wind and pressure responses in summer, but CLDMOD shows a year-round acceleration of the westerly winds and SLP drop in the high latitudes, and the opposite pattern in the middle latitudes. The precipitation response follows the seasonal movement of the westerly jet and sea level pressure trough. In the winter months, when the jet response is more equatorwards (and less zonally symmetric), the precipitation response is largest around 50°S. From late winter through summer, the precipitation response follows the wind and pressure responses polewards. Around April in LENS and May in CLDMOD, the wind and pressure responses abruptly shift equatorwards. This could be due to the seasonality of the forcing itself (Fig. 1), which is very weak in the autumn and early winter.

In contrast to the atmospheric circulation response, the temperature response is less seasonal (Fig. 10d). In LENS, temperature changes greater than 0.1 °C are largely confined to the polar latitudes. Cooling occurs across all latitudes from February to March, and warming occurs from April through December. This pattern bears no resemblance to the precipitation response. In CLDMOD, warming of 0.2° to 0.4 °C occurs in all months polewards of 45°S. Maxima in warming occur in the summer months between 50°S and 70°S, and near 60°S in the autumn months. This pattern is unlike the precipitation and atmospheric circulation patterns. Nonetheless, warming in this region, combined with sea ice loss, favors increased Antarctic precipitation (e.g. Wang et al. 2019). Is this small but significant warming in CLDMOD enough to explain the amplified precipitation response? Appealing first to basic principles, the Clausius-Clapeyron relation gives a temperature-precipitation slope of 9.7%/°C at ambient Antarctic temperatures (e.g. Palerme et al. 2016). With an average warming in our domain of ~ 0.25 °C, applying that slope yields a precipitation increase of just 2–3%, lower than the 7–8% increase that actually occurs. In the LENS ensemble, some ensemble members show annual mean cooling, yet all members show increased Antarctic precipitation. The ensemble mean shows near-zero annual mean surface temperature response on the AIS. Therefore, the temperature-precipitation slope in LENS cannot be used to predict the precipitation response in CLDMOD based on the CLDMOD temperature response. Given the close association of the precipitation response to the atmospheric circulation response in both CLDMOD and LENS, and the inability for the temperature response to explain the precipitation response by Clausius–Clapeyron scaling arguments, we conclude that the precipitation responses are primarily driven by atmospheric dynamics. As discussed below, future experiments with a water isotope-enabled version of CESM, combined with a "dynamical adjustment" approach, should help to more explicitly resolve this issue of thermodynamic versus dynamic controls on the precipitation response.

3.5 Shortwave feedbacks in CLDMOD and their role in the jet shift

Why does the surface and the atmosphere above warm more in CLDMOD than LENS, and why is the dynamical response stronger? By experiment design, we already know that the ultimate answer is because of the modified shallow convection scheme in CLDMOD. In this final section of results, we consider the processes that lead to more warming and a stronger jet shift in the CLDMOD experiment. Tropospheric warming in the present-day ozone experiments compared to pre-industrial may come directly from the small positive radiative forcing of tropospheric ozone gain (Cionni et al. 2011). Additional warming at Southern Ocean latitudes is caused by a variety of processes that are tied to the poleward shift and strengthening of the jet. These include horizontal Ekman heat transport, sea ice loss, entertainment of relatively warm at depth into the ocean mixed layer at high latitudes, and shallower mixed layers in the middle latitudes (e.g. Bitz and Polvani 2012). These processes operate in both the LENS and CLDMOD experiments, with slightly greater magnitude in CLDMOD due in part to the stronger wind responses.

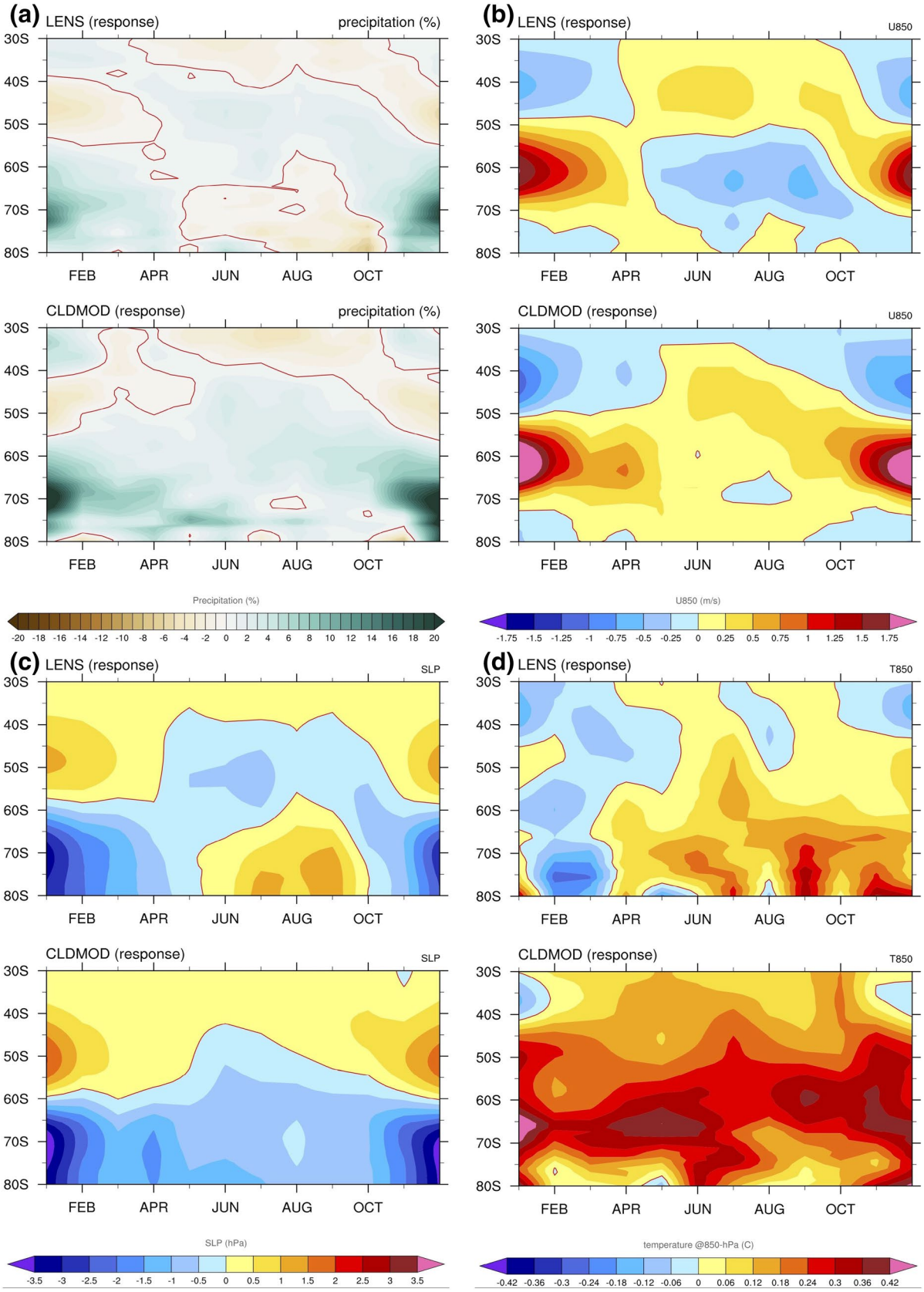

Fig. 10 Zonal-mean responses to ozone depletion as a function of month and latitude (30-80S) in LENS and CLDMOD for: **a** precipitation; **b** 850-hPa zonal wind; **c** sea level pressure; **d** 850-hPa temperature. The zero contour is outlined in red

The biggest differentiator of the CLDMOD and LENS versions of the experiments is the shortwave cloud feedback. Using the approximate partial radiative perturbation (APRP) methodology of Taylor et al. (2007), we evaluate shortwave feedbacks in both experiments. Table 3 shows the values of the shortwave cloud, surface albedo and total shortwave feedbacks globally and for the Southern Ocean latitudes of 40°S–70°S. The total includes shortwave noncloud feedbacks, which we do not focus on because of the potential for forcing and response to be mixed, owing to the strong shortwave perturbation caused by ozone depletion. In LENS, the sum of the shortwave feedbacks is zero W/m^2 globally and − 5.4 W/m^2 for the Southern Ocean latitudes; and the shortwave cloud feedback is − 0.47 W/m^2 globally and − 3.4 W/m^2 over the Southern Ocean. In contrast, CLDMOD has a positive shortwave cloud feedback both globally and over the Southern Ocean. This leads to a positive, global-mean total shortwave feedback of 1.21 W/m^2. The significance of the less negative shortwave cloud feedback in CLDMOD is underscored by the separation between the two ensembles in the zonal mean (Fig. 9d). For the latitudes 40°S to 55°S, every CLDMOD ensemble member exhibits a positive shortwave cloud feedback, while every LENS ensemble member shows a negative shortwave cloud feedback. The ensemble-mean responses, mapped in Fig. 11a, b, show a marked contrast between the shortwave cloud feedbacks in LENS and CLDMOD.

The differences in the shortwave cloud feedbacks are explained to first order by changes in cloud phase. As warming occurs, cloud ice is converted to cloud liquid, brightening the clouds and reflecting more incoming shortwave radiation back to space. Since CLDMOD has more cloud liquid in its mean state, there is less conversion of cloud ice to liquid as the climate warms. Figure 11a, c confirm that total cloud liquid increases in LENS over the same latitudes that the shortwave cloud feedback is negative. At the same time, CLDMOD shows (Fig. 11d) a mixed signal of either weak increases in cloud liquid or decreases in cloud liquid. Note that this cloud liquid diagnostic does not differentiate between changes in total cloud amount and changes in cloud liquid to ice ratios within the clouds themselves. Decreases in cloud amount may explain the existence of a positive shortwave cloud feedback in CLDMOD. These processes are diagnosed in detail by Frey and Kay (2018) in the context of doubled CO_2 experiments with the same models that we are using here. They found that warming of the ocean surface increases evaporation and low-level moisture, maintaining or increasing relative humidity. However, an increase in turbulent mixing across the top of boundary layer entrains dry air from the free troposphere into the boundary layer, reducing cloud fraction and liquid water path. We refer readers to Frey and Kay (2018) for additional discussion of the mechanisms involved in shortwave cloud feedbacks and the differences between CLDMOD and LENS.

Table 3 Global-mean, annual-mean, ensemble-mean values of shortwave feedbacks in the CLDMOD and LENS ozone experiments

Experiment	Total	Surface albedo	Shortwave cloud
CLDMOD	1.2 {1.4}	0.71 {2.6}	0.6 {0.76}
LENS	0.0 {− 5.4}	0.71 {1.8}	− 0.5 {− 3.4}

The total includes estimates of the shortwave noncloud feedback (not shown; see text for discussion). Values in W/m^2. The shortwave feedbacks for the 40°S–70°S region is shown in brackets

Are the more positive shortwave cloud feedbacks in CLDMOD responsible for the stronger poleward jet shift? In a sense, our results are related to a growing body of studies that associates the magnitude of poleward jet shifts with the strength of shortwave cloud feedbacks (e.g. Ceppi et al. 2012; Ceppi and Hartmann 2016; Ceppi and Shepherd 2017; Voigt and Shaw 2016; Li et al. 2019). One key difference is that the chief agent of the jet shift in our experiments is polar stratospheric cooling (drive by ozone loss) rather than middle and upper tropospheric warming in the tropics and mid-latitudes (driven by increased atmospheric CO_2 concentration). Still, we see an association between shortwave feedbacks and poleward jet shifts: The model with more positive shortwave feedbacks in the Southern hemisphere extratropics has a stronger poleward jet shift. This is actually a surprising result: the jet shifts more polewards in CLDMOD despite the changes in the shortwave cloud feedbacks, not because of them. Why? In CLDMOD, the pattern of zonal-mean shortwave cloud feedbacks damps the meridional gradients of absorbed shortwave radiation and temperature rather than strengthening them. In Fig. 9f, we can see that the negative shortwave feedback in the mid latitudes in LENS switches sign to positive in CLDMOD, while the positive shortwave feedback in the tropics in LENS is neutral in CLDMOD. In CLDMOD, there is greater warming in the high southern latitudes relative to the tropics, weakening the meridional temperature gradient. All else being equal, this would tend to weaken the jet shift. However, as can be seen by comparing Fig. 3a with e, the amount of near-surface, zonal-mean warming in CLDMOD is not enough to substantially weaken the meridional gradient of the control climate. Nonetheless, there is a small tropospheric warming in the deep tropics (Fig. 3e) that acts to enhance the temperature gradient, but this is not explained by shortwave cloud feedbacks (Fig. 9d).

The reasons for the stronger jet response in CLDMOD, we suggest, lie in the upper tropospheric zonal-mean temperature structure of the control run. As noted earlier, the control run of CLDMOD has a stronger equator-to-pole temperature gradient and increased tropopause slope relative to the LENS control. This implies increased baroclinic instability in the midlatitude upper troposphere, which acts

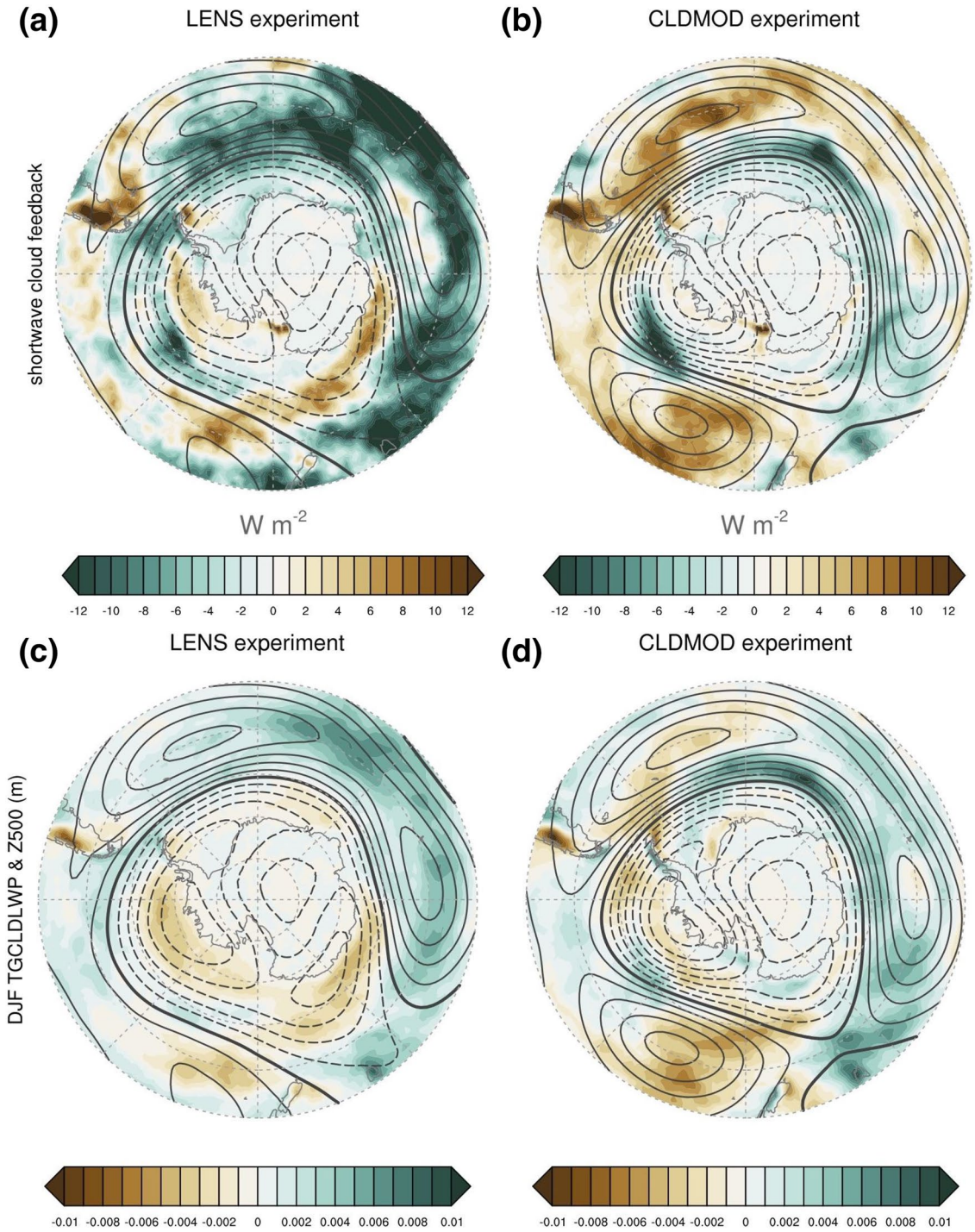

Fig. 11 Responses of annual-mean shortwave cloud feedback (colorscale in top panels; W m^{-2} K^{-1}) and total cloud liquid water path (colorscale in bottom panels; kg m^{-2}) in DJF to ozone depletion in LENS and CLDMOD. The overlaid contours are Z500, as in Fig. 6

to increase the poleward shift of the jet. The increase in the zonal wind speed near the tropopause (Fig. 3b) also implies an increase in eddy phase speed, which would confine eddies to higher latitudes and converge momentum more polewards (e.g. Lu et al. 2008). In addition, the results (Fig. 3e) show evidence for an increase in static stability in the tropics and subtropics, and an increase in tropopause height, two additional mechanisms that are involved in poleward jet shifts (e.g. Li et al. 2019; Lorenz and DeWeaver 2007; Lu et al. 2008; Kidston et al. 2011). In summary, our results suggest that the difference in the jet response between CLDMOD and LENS is not due to

shortwave feedbacks, but rather due to the different mean states of the two models.

4 Summary and discussion

The results presented here demonstrate three major aspects of the response of Antarctic precipitation to stratospheric ozone depletion in the context of a comprehensive Earth system model (CESM1): (1) Antarctic precipitation increases significantly in response to stratospheric ozone depletion, confirming previous studies; (2) this response is largely driven by atmospheric dynamics; and (3) the magnitude of the precipitation response is highly sensitive to a parameterization change that improves the shortwave radiative properties of clouds over the Southern Ocean. On this latter point, the modified version of CESM1 (CLDMOD) shows an average precipitation increase of 109 Gt year^{-1} in response to ozone forcing, whereas the standard (LENS) version of CESM1 shows an increase of 34 Gt year^{-1}. The LENS response is similar to that reported by Lenaerts et al. (2018) in the "leave-one-out" historical experiments that they analyze, in which the ensemble with all forcings gains 38 Gt year^{-1} more snowfall than the ensemble with all forcings active except for ozone over 1986–2005. Results from our ozone loss experiments are more direct in that they do not rely on subtraction from an all forcing run to isolate the ozone signal. This avoids any nonlinearities that may arise when multiple forcings are convolved, but nonethesless does not take into account interactions between different types of forcing. Taken together, the two studies suggest that the ozone signal in Antarctic precipitation is largely insensitive to the experimental design chosen.

In light of the role of the AIS in sea level rise, the 109 Gt year^{-1} (~0.3 mm sea level equivalent) ozone-driven increase in Antarctic snowfall in CLDMOD is important. At face value, this number essentially matches the observed rate of mass loss from the AIS over 1992–2017 (IMBIE Team 2018). While it is just a coincidence that these numbers match, our experiments illustrate the potential for increased snowfall on the AIS to have a meaningful impact on Antarctic mass balance, therefore partially offsetting the ice sheet's sea level rise contributions. Recognizing the relevance of these numbers for the sea level rise problem, we encourage further efforts to determine the role of structural uncertainty in the Antarctic precipitation response to ozone, using a variety of independent models and methods. More observations, and observational syntheses such as that by Medley and Thomas (2019), are also needed both to confirm the signal of ozone depletion in historical snowfall trends, and to better quantify the role of SMB in the overall mass balance of the AIS. It is essential to note that snowfall is only part of the mass balance of the AIS, and that the potential impacts of ozone depletion on mass balance are not limited to increased snowfall. The stronger poleward jet shift in CLDMOD implies an increase in the delivery of relatively warm subsurface waters to the fringing ice shelves and outlet glaciers of the AIS, potentially increasing the rate of dynamic mass loss (e.g. Holland et al. 2019). The increased snowfall itself could also drive an increase in ice discharge and mass loss via steepening the elevation profile of ice sheet and increasing the driving stress, but this will act on a longer timescale than the snowfall response (Winkelmann et al. 2012). The nature of these coupled processes underscores an ongoing need for fully interactive ice sheet models within Earth system models.

The results point to a poleward shift of the eddy-driven jet as the primary mechanism that brings more precipitation to the AIS in both ozone depletion experiments. The precipitation response follows the jet response through the seasonal cycle. Both responses reach their maximum amplitude and poleward extent in austral summer, consistent with polar stratospheric ozone depletion as the main driver. In CLDMOD, the DJF jet shift is focused about two degrees more polewards than in LENS, associated with a more intense strengthening of the westerlies. The poleward jet shift is also evident year-round in CLDMOD, in contrast to the opposite-signed summer and winter responses in LENS. These two factors contribute to the greater than three-fold amplification of the annual-mean Antarctic precipitation response in CLDMOD. Evidence has also been presented that explains the more pronounced jet shift in CLDMOD. Although there is not a universally accepted, singular mechanism for poleward jet shifts, our results are consistent with many previous studies that tie jet shifts to the zonal-mean, meridional temperature gradient as well as an increase in static stability on the equatorward side of the jet. Specifically, CLDMOD has a stronger meridional temperature gradient in the mid latitude upper troposphere in its control climate. The meridional temperature gradient in the upper troposphere—lower stratosphere is strengthened even further when stratospheric ozone depletion is prescribed. While it is beyond the scope of this work to evaluate the specific wave-mean flow feedbacks involved, these results are consistent with an increase in eddy phase speed (e.g. Lu et al. 2008) and/or an increase in eddy length scale (Kidston et al. 2011) as the means by which more momentum is delivered to the jet on its poleward flank. In addition, CLDMOD shows evidence for increased static stability in the subtropics, marked by mid tropospheric warming (Fig. 3e). This may push eddy activity polewards, leading to a poleward shift of the eddy-driven jet (e.g. Lu et al. 2008).

We have purposely characterized the atmospheric circulation response to ozone depletion as a poleward shift of the jet, and not as a tendency towards the positive phase of the Southern Annular Mode (SAM; e.g. Thompson and

Wallace 2000). In most models, including the CESM1, the SAM is more correlated with jet strength than with jet position, but the degree of correlation varies across models and timescales (Swart et al. 2015). Disambiguating jet strength and jet position is important because these two kinematic features of the jet imply different impacts on the atmosphere–ocean-ice system (Bracegirdle et al. 2018). For Antarctic precipitation, the positive phase of the SAM has been associated with a net decrease (Medley and Thomas 2019), while, as seen here, a poleward shift of the jet is associated with a net increase. In geopotential height, a strengthening of the jet, as seen in the difference between the LENS and CLDMOD control simulations, is accompanied by only a weak stationary wave amplitude over the AIS, while a poleward shift, as seen in both the LENS and CLDMOD ozone experiments, is accompanied by a large-amplitude stationary wave over the continent. We caution future studies of the large-scale Southern Hemisphere atmospheric circulation and its impacts against equating the positive phase of the SAM with a poleward jet shift.

We have also considered the role of shortwave feedbacks in determining the different precipitation responses in CLDMOD and LENS. In CLDMOD, shortwave cloud feedbacks in the middle to high latitudes are more positive than in LENS, leading to greater warming. The enhanced warming in CLDMOD in our ozone loss experiments is consistent with results from both doubled CO_2 (Frey and Kay 2018) and transient 21st Century (Frey et al. 2017) experiments using the same model version. In our experiments, the more positive shortwave feedbacks and additional warming in CLDMOD compared to LENS are not sufficient to explain the amplified precipitation response. Using scaling arguments, we show that the warming in CLDMOD could at best explain a ~ 3% increase in Antarctic precipitation, less than half of the more than 7% increase that actually occurs.

Shortwave feedbacks could also play a role in the precipitation response via forcing latitudinal changes in jet position. However, compared to LENS, CLDMOD has more positive shortwave cloud feedbacks in the middle and high latitudes, and less positive feedbacks in the tropics, weakening the meridional temperature gradient and countering the poleward shift of the jet. While a number of studies have associated the magnitude of shortwave feedbacks with the magnitude of the jet shift (e.g. Ceppi et al. 2012; Ceppi and Hartmann 2016; Ceppi and Shepherd 2017; Voigt and Shaw 2016; Li et al. 2019), our results suggest that the initial distribution of shortwave energy could be more important for determining the jet response than the feedbacks. The question remains as to how this competition between the mean state and the feedbacks will play out in a 21st Century climate change scenario. Ozone recovery will replace ozone depletion as the main driver of the jet response in the high latitudes, while rising greenhouse gas concentrations will tend to push the jet polewards. In CLDMOD, the shortwave feedbacks in a 21st Century scenario should act to damp the jet shift to a greater extent than in the ozone experiments we have evaluated here. Future work will be aimed at addressing these issues using ensembles of 20th and 21st Century experiments with both CLDMOD and LENS.

The relative dominance of the dynamic mechanism on Antarctic precipitation that we have seen in these experiments may be weakened in a 21st Century climate change scenario if warming is of greater magnitude, and the poleward jet shift is of lesser magnitude. Still, our results suggest that dynamics are more important for Antarctic precipitation projections than is commonly assumed. Towards this end, separation of dynamic and thermodynamic mechanisms in Antarctic precipitation may require additional diagnostic tools. These may include a dynamical adjustment approach (e.g. Guo et al. 2019) and/or using water-isotope enabled versions of the model (Brady et al. 2019). With respect to the latter, a poleward shift in the dominant source region of Antarctic precipitation should be recorded in strong isotopic enrichment, while a modest warming of a stationary source region may barely be detectable in the isotopic ratios, but could be reflected in the deuterium excess (Bailey et al. 2019). From water tagging experiments with the CESM1 by Singh et al. (2016), we know that the mean moisture source region for the coastal areas of the AIS where precipitation increases the most is generally between 44°S and 48°S. The relatively distant source region, and the relative dominance of large-scale atmospheric dynamics, suggests that future Antarctic precipitation trends may not be as strongly tied to sea ice retreat and coastal warming as some studies have suggested (Agosta et al. 2015; Bracegirdle et al. 2015). Finally, atmospheric dynamics may prove to be very important in models with finer horizontal resolution, which better resolve the topography of coastal Antarctica and its steep orographic precipitation gradients (e.g. Genthon et al. 2009).

5 Conclusion

Our experiments demonstrate that polar stratospheric ozone depletion drives a poleward shift of westerly jet and storm tracks, leading to a significant increase of precipitation on the AIS. This magnitude of this impact, however, is strongly sensitive to the mean state of an Earth system model. Reducing long-standing biases in shortwave cloud forcing cools the Southern Ocean and warms the tropics, creating a strong meridional temperature gradient, especially in the midlatitude upper troposphere—lower stratosphere. This in turn sets up a more robust poleward shift of the jet when the model is forced with realistic levels of stratospheric ozone depletion. While the standard version of the model exhibits a precipitation increase on

the Antarctic Ice Sheet of 34 gigatons year^{-1}; the cloud-modified version shows an increase of 109 Gt year^{-1}. The cloud-modified version also shows significant differences in shortwave cloud feedbacks, which in a 21st Century climate change scenario could affect both the amount of warming over the Southern Ocean and the strength of the jet shift. Determining the role of structural uncertainty in 21st Century projections of Antarctic precipitation is of utmost importance given the central role of the AIS in sea level rise.

Acknowledgments The CESM1 Large Ensemble control experiment is available from the Climate Data Gateway at NCAR. The "CLD-MOD" control simulation, published in a previous study, is available on the HPSS at NCAR. The "low ozone" experiments are available through the authors. DPS acknowledges salary and travel support from National Science Foundation (NSF) grant 1643484. JEK acknowledges support from NSF grant 163493. We would also like to acknowledge high-performance computing support from Cheyenne (https://doi.org/10.5065/d6rx99hx) provided by NCAR's Computational and Information Systems Laboratory, sponsored by the National Science Foundation. This material is based upon work supported by the National Center for Atmospheric Research, which is a major facility sponsored by the National Science Foundation under Cooperative Agreement no. 1852977. The authors thank Dr. Clara Deser for discussion of these results and for a constructive review of a draft version of this manuscript. The authors also thank two anonymous reviewers for constructive reviews.

References

Agosta C, Fettweis X, Datta R (2015) Evaluation of the CMIP5 models in the aim of regional modelling of the Antarctic surface mass balance. Cryosph 9:2311–2321. https://doi.org/10.5194/tc-9-2311-2015

Bailey A, Singh HKA, Nusbaumer J (2019) Evaluating a moist isentropic framework for poleward moisture transport: implications for water isotopes over Antarctica. Geophys Res Lett 46:7819–7827. https://doi.org/10.1029/2019GL082965

Bitz CM, Polvani LM (2012) Antarctic climate response to stratospheric ozone depletion in a fine resolution ocean climate model. Geophys Res Lett 39(20)

Bracegirdle TJ, Stephenson DB, Turner J, Phillips T (2015) The importance of sea ice area biases in 21st century multimodel projections of Antarctic temperature and precipitation. Geophys Res Lett 42(10832–10):839. https://doi.org/10.1002/2015GL067055

Bracegirdle TJ, Hyder P, Holmes CR (2018) CMIP5 diversity in southern westerly jet projections related to historical sea ice area: strong link to strengthening and weak link to shift. J Clim 31(1):195–211

Brady E, Stevenson S, Bailey D et al (2019) The connected isotopic water cycle in the community earth system model version 1. J Adv Model Earth Syst 11:2547–2566. https://doi.org/10.1029/2019MS001663

Ceppi P, Hwang Y-T, Frierson DMW, Hartmann DL (2012) Southern Hemisphere jet latitude biases in CMIP5 models linked to shortwave cloud forcing. Geophys Res Lett. https://doi.org/10.1029/2012GL053115

Ceppi P, Hartmann DL (2016) Clouds and the atmospheric circulation response to Warming. J Clim 29:783–799. https://doi.org/10.1175/JCLI-D-15-0394.1

Ceppi P, Shepherd TG (2017) Contributions of climate feedbacks to changes in atmospheric circulation. J Clim 30:9097–9118. https://doi.org/10.1175/JCLI-D-17-0189.1

Cionni I, Eyring V, Lamarque JF et al (2011) Ozone database in support of CMIP5 simulations: results and corresponding radiative forcing. Atmos Chem Phys 11:11267–11292. https://doi.org/10.5194/acp-11-11267-2011

Eyring V, Arblaster JM, Cionni I et al (2013) Long-term ozone changes and associated climate impacts in CMIP5 simulations. J Geophys Res Atmos 118:5029–5060. https://doi.org/10.1002/jgrd.50316

Ferreira D, Marshall J, Bitz CM et al (2015) Antarctic ocean and sea ice response to ozone depletion: a two-time-scale problem. J Clim 28:1206–1226. https://doi.org/10.1175/JCLI-D-14-00313.1

Frey WR, Kay JE (2018) The influence of extratropical cloud phase and amount feedbacks on climate sensitivity. Clim Dyn 50:3097–3116. https://doi.org/10.1007/s00382-017-3796-5

Frey WR, Maroon EA, Pendergrass AG, Kay JE (2017) Do Southern Ocean cloud feedbacks matter for 21st century warming? Geophys Res Lett 44:12447–12456. https://doi.org/10.1002/2017GL076339

Fyke J, Lenaerts JTM, Wang H (2017) Basin-scale heterogeneity in Antarctic precipitation and its impact on surface mass variability. Cryosph 11:2595–2609. https://doi.org/10.5194/tc-11-2595-2017

Genthon C, Krinner G, Castebrunet H (2009) Antarctic precipitation and climate-change predictions: horizontal resolution and margin vs plateau issues. Ann Glaciol 50:55–60. https://doi.org/10.3189/172756409787769681

Gillett NP, Thompson DWJ (2003) Simulation of recent southern hemisphere climate change. Science 302(5643):273–275

Guo R, Deser C, Terray L, Lehner F (2019) Human influence on winter precipitation trends (1921–2015) over North America and Eurasia revealed by dynamical adjustment. Geophys Res Lett 46:3426–3434. https://doi.org/10.1029/2018GL081316

Holland PR, Bracegirdle TJ, Dutrieux P et al (2019) West Antarctic ice loss influenced by internal climate variability and anthropogenic forcing. Nat Geosci 12:718–724. https://doi.org/10.1038/s41561-019-0420-9

Hurrell JW, Holland MM, Gent PR et al (2013) The community earth system model: a framework for collaborative research. Bull Am Meteorol Soc 94:1339–1360. https://doi.org/10.1175/BAMS-D-12-00121.1

Jones ME, Bromwich DH, Nicolas JP et al (2019) Sixty years of widespread warming in the southern middle and high latitudes (1957–2016). J Clim 32:6875–6898. https://doi.org/10.1175/JCLI-D-18-0565.1

Kay JE, Deser C, Phillips A et al (2014) The Community Earth System Model (CESM) large ensemble project: a community resource for studying climate change in the presence of internal climate variability. Bull Am Meteorol Soc. https://doi.org/10.1175/BAMS-D-13-00255.1

Kay JE, Wall C, Yettella V et al (2016) Global climate impacts of fixing the southern ocean shortwave radiation bias in the Community Earth System Model (CESM). J Clim 29:4617–4636. https://doi.org/10.1175/JCLI-D-15-0358.1

Kidston J, Vallis GK, Dean SM et al (2011) Can the increase in the eddy length scale under global warming cause the poleward shift of the jet streams? J Clim 24:3764–3780. https://doi.org/10.1175/2010JCLI3738.1

Kostov Y, Marshall J, Hausmann U et al (2016) Fast and slow responses of Southern Ocean sea surface temperature to SAM in coupled climate models. Clim Dyn. https://doi.org/10.1007/s00382-016-3162-z

Lenaerts JTM, van den Broeke MR, van de Berg WJ et al (2012) A new, high-resolution surface mass balance map of Antarctica (1979–2010) based on regional atmospheric climate modeling. Geophys Res Lett. https://doi.org/10.1029/2011GL050713

Lenaerts JTM, Vizcaino M, Fyke J et al (2016) Present-day and future Antarctic ice sheet climate and surface mass balance in the Community Earth System Model. Clim Dyn 47:1367–1381. https://doi.org/10.1007/s00382-015-2907-4

Lenaerts JTM, Fyke J, Medley B (2018) The signature of ozone depletion in recent Antarctic precipitation change: a study with the community earth system model. Geophys Res Lett 45:12931–12939. https://doi.org/10.1029/2018GL078608

Lenaerts JTM, Medley B, Broeke MR, Wouters B (2019) Observing and modeling ice sheet surface mass balance. Rev Geophys 57(2):376–420

Li Y, Thompson DWJ, Bony S et al (2019) Thermodynamic control on the poleward shift of the extratropical jet in climate change simulations: the role of rising high clouds and their radiative effects. J Clim 32:917–934. https://doi.org/10.1175/JCLI-D-18-0417.1

Lorenz DJ, DeWeaver ET (2007) Tropopause height and zonal wind response to global warming in the IPCC scenario integrations. J Geophys Res: Atmos 112(D10)

Lu J, Chen G, Frierson DMW et al (2008) Response of the zonal mean atmospheric circulation to El Niño versus global warming. J Clim 21:5835–5851. https://doi.org/10.1175/2008JCLI2200.1

Marsh DR, Mills MJ, Kinnison DE et al (2013) Climate change from 1850 to 2005 simulated in CESM1 (WACCM). J Clim 26:7372–7391. https://doi.org/10.1175/JCLI-D-12-00558.1

Medley B, Thomas ER (2019) Increased snowfall over the Antarctic Ice Sheet mitigated twentieth-century sea-level rise. Nat Clim Chang 9:34–39. https://doi.org/10.1038/s41558-018-0356-x

Monaghan AJ, Bromwich DH, Fogt RL et al (2006) Insignificant change in Antarctic snowfall since the International Geophysical Year. Science 313:827–831. https://doi.org/10.1126/science.1128243

Nicolas JP, Bromwich DH (2014) new reconstruction of antarctic near-surface temperatures: multidecadal trends and reliability of Global reanalyses*,+. J Clim 27:8070–8093. https://doi.org/10.1175/JCLI-D-13-00733.1

Palerme C, Genthon C, Claud C et al (2016) Evaluation of current and projected Antarctic precipitation in CMIP5 models. Clim Dyn. https://doi.org/10.1007/s00382-016-3071-1

Polvani LM, Waugh DW, Correa GJP, Son S-W (2011) Stratospheric ozone depletion: the main driver of twentieth-century atmospheric circulation changes in the southern hemisphere. J Clim 24:795–812. https://doi.org/10.1175/2010JCLI3772.1

Previdi M, Polvani LM (2016) Anthropogenic impact on Antarctic surface mass balance, currently masked by natural variability, to emerge by mid-century. Environ Res Lett 11:094001. https://doi.org/10.1088/1748-9326/11/9/094001

Sallée JB, Speer KG, Rintoul SR (2010) Zonally asymmetric response of the Southern Ocean mixed-layer depth to the Southern Annular Mode. Nat Geosci 3:273–279. https://doi.org/10.1038/ngeo812

Sallée J-B, Shuckburgh E, Bruneau N et al (2013) Assessment of Southern Ocean water mass circulation and characteristics in CMIP5 models: historical bias and forcing response. J Geophys Res Ocean 118:1830–1844. https://doi.org/10.1002/jgrc.20135

Schneider DP, Reusch DB (2016) Antarctic and Southern Ocean surface temperatures in CMIP5 models in the context of the surface energy budget. J Clim. https://doi.org/10.1175/JCLI-D-15-0429.1

Schneider DP, Deser C, Fan T (2015) Comparing the impacts of tropical SST variability and Polar stratospheric ozone loss on the Southern Ocean westerly winds*. J Clim 28(23):9350–9372

Singh HA, Bitz CM, Nusbaumer J, Noone DC (2016) A mathematical framework for analysis of water tracers: part 1: development of theory and application to the preindustrial mean state. J Adv Model Earth Syst 8:991–1013. https://doi.org/10.1002/2016MS000649

Steig EJ, Schneider DP, Rutherford SD et al (2009) Warming of the Antarctic ice-sheet surface since the 1957 international geophysical year. Nature 457:459–462. https://doi.org/10.1038/nature07669

Swart NC, Fyfe JC, Gillett N et al (2015) Comparing trends in the southern annular mode and surface westerly jet. J Clim 28:8840–8859. https://doi.org/10.1175/JCLI-D-15-0334.1

Taylor KE, Crucifix M, Braconnot P et al (2007) Estimating shortwave radiative forcing and response in climate models. J Clim 20:2530–2543. https://doi.org/10.1175/JCLI4143.1

Team IMBIE (2018) Mass balance of the Antarctic Ice Sheet from 1992 to 2017. Nature 558:219–222. https://doi.org/10.1038/s41586-018-0179-y

Thomas ER, van Wessem JM, Roberts J et al (2017) Regional Antarctic snow accumulation over the past 1000 years. Clim Past 13:1491–1513. https://doi.org/10.5194/cp-13-1491-2017

Thompson DWJ, Wallace JM (2000) Annular modes in the extratropical circulation. Part I: month-to-month variability. J Clim 13:1000–1016. https://doi.org/10.1175/1520-0442(2000)013<1000:AMITEC>2.0.CO;2

Trenberth KE, Fasullo JT (2010) Simulation of present-day and twenty-first-century energy budgets of the southern oceans. J Clim 23:440–454. https://doi.org/10.1175/2009JCLI3152.1

Vallis GK, Zurita-Gotor P, Cairns C, Kidston J (2015) Response of the large-scale structure of the atmosphere to global warming. Q J R Meteorol Soc 141(690):1479–1501

Voigt A, Shaw TA (2016) Impact of regional atmospheric cloud radiative changes on shifts of the extratropical jet stream in response to global warming. J Clim 29:8399–8421. https://doi.org/10.1175/JCLI-D-16-0140.1

Wang H, Fyke J, Lenaerts J, et al (2019) Influence of Sea Ice Anomalies on Antarctic Precipitation Using Source Attribution. Cryosph Discuss. https://doi.org/10.5194/tc-2019-69

Winkelmann R, Levermann A, Martin MA, Frieler K (2012) Increased future ice discharge from Antarctica owing to higher snowfall. Nature 492:239–242. https://doi.org/10.1038/nature11616

Zunz V, Goosse H, Massonnet F (2013) How does internal variability influence the ability of CMIP5 models to reproduce the recent trend in Southern Ocean sea ice extent? Cryosph Discuss 7:451–468. https://doi.org/10.5194/tc-7-451-2013